Sustainable Cities and Society 83 (2022) 103975

Contents lists available at ScienceDirect

Sustainable Cities and Society

journal homepage: www.elsevier.com/locate/scs

A microgrid formation-based restoration model for resilient distribution systems using distributed energy resources and demand response programs

Mohammad Amin Gilani [a], Reza Dashti [b], Mostafa Ghasemi [a], Mohammad Hassan Amirioun [c], Miadreza Shafie-khah [d,*]

[a] Centre of Excellence for Power System Automation and Operation, Department of Electrical Engineering, Iran University of Science and Technology, Tehran, Iran
[b] Department of New Technologies, Iran University of Science and Technology, Tehran, Iran
[c] Department of Electrical Engineering, Shahreza Campus, University of Isfahan, Iran
[d] School of Technology and Innovations, University of Vaasa, Vaasa, Finland

ARTICLE INFO

Keywords:
Resilience
Distribution system restoration
Demand response programs
Distributed energy resources (DERs)
Microgrids (MGs)
Multi-objective optimization

ABSTRACT

In recent years, resilience enhancement of electricity distribution systems has attracted much attention due to the significant rise in high-impact rare (HR) natural event outages. The performance of the post-event restoration after an HR event is an effective measure for a resilient distribution network. In this paper, a multi-objective restoration model is presented for improving the resilience of an electricity distribution network. In the first objective function, the load shedding in the restoration process is minimized. As the second objective function, the restoration cost is minimized which contradicts the first objective function. Microgrid (MG) formation, distributed energy resources (DERs), and demand response (DR) programs are employed to create the necessary flexibility in distribution network restoration. In the proposed model, DERs include fossil-fueled generators, renewable wind-based and PV units, and energy storage system while demand response programs include transferable, curtailable, and shiftable loads. The proposed multi-objective model is solved using ε-constraint method and the optimal solution is selected using the fuzzy satisfying method. Finally, the proposed model was successfully examined on 37-bus and 118-bus distribution networks. Numerical results verified the efficacy of the proposed method as well.

1. Introduction

In recent years, inevitable natural disasters have become more severe and frequent due to climate change. These HR events lead to significant growth in power outage intensity and frequency. Among recent experiences of HR weather events causing power outages in distribution systems (Najafi et al., 2018; Panteli et al., 2017), hurricane Harvey can be mentioned which made landfall on Texas and Louisiana in August 2017 and left around 0.3 million of customers in a power outage throughout Texas for 14 days. The worldwide concerns on adverse impacts of HR weather events on critical infrastructures have led to the introduction of the concept of power system resilience. Resilience enhancement strategies aim at improving the power system response and restoration against HR events (Gholami et al., 2018).

Many researchers have studied distribution system restoration which aims to recover critical loads by resource rescheduling and structure reconfiguration after the incident. However during HR events, the upstream network may be unavailable and thus the distribution network should be operated in the islanded mode. In such conditions, traditional operational strategies cannot guarantee the continuity of power delivery (Hemmati et al., 2021). Distributed generators and smart grid technologies such as demand response programs can enhance the distribution system resilience by increasing the load restoration capability.

With the high penetration of DGs, MG formation is an effective operational strategy to restore critical loads as major faults occur in distribution systems. Optimal methods based on heuristic search (Bajpai et al., 2016; Sedzro et al., 2018; Xu et al., 2016; Zadsar et al., 2017) and mathematical programming (Alizadeh et al., 2020; Biswas et al., 2021; Gilani et al., 2020; Momen et al., 2020, 2021; Sedzro et al., 2017; Zhu et al., 2020) were used for MG formation problem in the resilient distribution systems. In (Bajpai et al., 2016), a methodology based on the graph-theoretic method and Choquet integral was introduced for MG formation to quantify the distribution system resilience during extreme contingencies. In Sedzro et al. (2018), a heuristic approach was proposed that allows solving the post-event MG formation problem for

* Corresponding author.
E-mail address: mshafiek@uwasa.fi (M. Shafie-khah).

https://doi.org/10.1016/j.scs.2022.103975
Received 22 February 2022; Received in revised form 23 May 2022; Accepted 31 May 2022
Available online 1 June 2022

Nomenclature

Indices and Sets

i,r	set of buses, ranging from 1 to N^{bus}
j	set of buses with control capability
q	set of buses without control capability
sh	set of buses with shifting capability (sha)
cu	set of buses with curtailing capability (cur)
tr	set of buses with transfer capability (tra)
dg	set of functional DGs, ranging from 1 to N^{dg}
mdg	set of functional master DGs, ranging from 1 to N^{mdg}
pv	set of functional photovoltaic units, ranging from 1 to N^{pv}
w	set of wind turbines, ranging from 1 to N^{w}
e	set of energy storage units, ranging from 1 to N^{e}
i^{DG}	set of buses with DG
i^{MDG}	set of buses with master DG
i^{sor}	set of buses with photovoltaic unit
i^{wnd}	set of buses with wind turbine
i^{ES}	set of buses with energy storage unit
i^{From}	set of initial buses of line l
i^{To}	set of terminal buses of line l
L	set of lines and tie lines, ranging from 1 to N^{L}
L^{nots}	set of lines without switch
m	set of formable microgrids, ranging from 1 to N^{mdg}
t	index of the post-event restoration time
ψ	set of scenarios, ranging from 1 to N^{ψ}
θ^{max}	maximum limit of the voltage angle
τ	set of time slots for transferable demand response, ranging from 1 to 24

Parameters

DGs	Xxxxxxxx
N^{dg}	number of functional DG units
N^{mdg}	number of functional master DG units
$P_{dg}^{DG,max}$	maximum active power limit (kW) of DG
$Q_{dg}^{DG,max}$	maximum reactive power limit (kVar) of DG
$Q_{dg}^{DG,min}$	minimum reactive power limit (kVar) of DG
$Pr_{dg,\psi,t}^{DG}$	the price of generated power ($/kWh) by the DG
PVs	Xxxxx
N^{pv}	number of functional photovoltaic units
$P_{pv,\psi,t}^{sor,max}$	maximum power limit (kW) of solar unit
$Pr_{pv,\psi,t}^{sor}$	the price of generated power ($/kWh) by the PV
WTs	Xxxxx
N^{w}	number of functional wind turbine units
$P_{w,\psi,t}^{wnd,max}$	maximum power limit (kW) of wind turbine unit
$Pr_{w,\psi,t}^{wnd}$	the price of generated power ($/kWh) by the WT
ESs	Xxxxx
N^{e}	number of functional energy storage units
SOC_{e}^{max}	maximum SOC (kWh) of storage units
SOC_{e}^{min}	minimum SOC (kWh) of storage units
$SOC_{e}^{initial}$	initial SOC (kWh) of storage units
$RT_{e}^{ch,max}$	maximum charge rate (kW/h) of storage units
$RT_{e}^{dch,max}$	maximum discharge rate (kW/h) of storage units
η_{e}^{ES}	efficiency of storage units
$Pr_{e,\psi,t}^{ES}$	the price of generated power ($/kWh) by the ES

Demand response

$LPF^{sha,up}$	coefficient for determining the maximum power transferred to increase the load in the shiftable model (kW)
$LPF^{sha,down}$	coefficient for determining the maximum power transferred to decrease the load in the shiftable model (kW)
$Pr_{sh,\psi,t}^{sha}$	price ($/kWh) of using shiftable load scheme for bus *sh* at time *t*
$LPF^{cur,up}$	coefficient for determining the maximum power transferred to increase the load in the curtailable model (kW)
$LPF^{cur,down}$	coefficient for determining the maximum power transferred to decrease the load in the shiftable model (kW)
$Pr_{cu,\psi,t}^{cur}$	price ($/kWh) of using curtailable load scheme for bus *cu* at time *t*
$LPF^{tra,up}$	coefficient for determining the maximum power transferred to increase the load in the transferable model (kW)
$LPF^{tra,down}$	coefficient for determining the maximum power transferred to decrease the load in the shiftable model (kW)
$Pr_{tr,\psi,t}^{tra}$	price ($/kWh) of using transferable load scheme for bus *tr* at time *t*
$Pr_{q,t}^{shed}$	load shedding price ($/kWh) for bus *q* at time *t*

Line & bus

N^{bus}	number of buses
$P_{i,\psi,t}^{load,pre}$	predicted active power (kW) of load *i*
$F_{i,\psi,t}^{pr}$	priority of load *i*
$P_{l}^{flow,max}$	active power flow limit (kW) of line *l*
$Q_{l}^{flow,max}$	reactive power flow limit (kVar) of line *l*
R_l, X_l	resistance and reactance (Ω) of line *l*
N^{L}	number of lines and tie lines
$Z1^{l}, Z2^{l}$	electrical characteristics of line *l*
$Sign_{i,l,\psi}$	connection sign between bus *i* and line *l*: −1 if bus *i* is the initial bus of line *l*; 1 otherwise.
BigM	a big number
ε_{ψ}	probability of each scenario

Variables

DGs	Xxxxx
$P_{dg,m,\psi,t}^{DG}$	active output power (kW) of DG in microgrid *m*
$Q_{dg,m,\psi,t}^{DG}$	reactive output power (kVar) of DG in microgrid *m*
$Cost_{dg,\psi,t}^{DG}$	DG operation cost ($)
PVs	Xxxxx
$P_{pv,m,\psi,t}^{sor}$	active output power (kW) of solar cell unit in microgrid *m*
$Cost_{pv,\psi,t}^{sor}$	PV operation cost ($)
WTs	Xxxxx
$P_{w,m,\psi,t}^{wnd}$	active output power (kW) of wind turbine in microgrid *m*
$Cost_{w,\psi,t}^{wnd}$	WT operation cost ($)
ESs	Xxxxx
$P_{e,m,\psi,t}^{ES,ch}, P_{e,m,\psi,t}^{ES,dch}$	charging and discharging power (kW) of ES unit in microgrid *m*
$P_{e,m,\psi,t}^{SOC}$	SOC (kWh) of ES unit in microgrid *m*
$\gamma_{e,m,\psi,t}^{ES}$	binary variable: status of ES unit in microgrid *m*
$Cost_{e,\psi,t}^{ES}$	ES operation cost ($)

Demand response

$P_{sh,m,\psi,t}^{sha}$	active power (kW) of shiftable load scheme for bus *sh* in microgrid *m*
$P_{sh,\psi,t}^{sha,up}$	increasing power transfer of shiftable load scheme for bus *sh*
$P_{sh,\psi,t}^{sha,down}$	decreasing power transfer of shiftable load scheme for bus *sh*
$\delta_{sh,\psi,t}^{sha,up}$	binary variable indicating whether increasing power transfer has been performed on the bus
$\delta_{sh,\psi,t}^{sha,down}$	binary variable indicating whether decreasing power transfer has been performed on the bus

$P^{cur}_{cu,m,\psi,t}$ active power (kW) of curtailable load scheme for bus *cu* in microgrid *m*
$P^{cur,up}_{cu,\psi,t}$ increasing power transfer of curtailable load scheme for bus *cu*
$P^{cur,down}_{cu,\psi,t}$ decreasing power transfer of curtailable load scheme for bus *cu*
$\delta^{cur,up}_{cu,\psi,t}$ binary variable indicating whether increasing power transfer has been performed on the bus
$\delta^{cur,down}_{cu,\psi,t}$ binary variable indicating whether decreasing power transfer has been performed on the bus
$P^{tra}_{tr,m,\psi,t}$ active power (kW) of transferable load scheme for bus *tr* in microgrid *m*
$P^{tra,up}_{tr,\psi,t}$ increasing power transfer of transferable load scheme for bus *tr*
$P^{tra,down}_{tr,\psi,t}$ decreasing power transfer of transferable load scheme for bus *tr*
$\delta^{tra,up}_{tr,\psi,t}$ binary variable indicating whether increasing power transfer has been performed on the bus
$\delta^{tra,down}_{tr,\psi,t}$ binary variable indicating whether decreasing power transfer has been performed on the bus
$P^{shed}_{i,m,\psi,t}$ load shedding (kW) of load *i* in microgrid *m*
$Cost^{sha}_{sh,\psi,t}$ load control cost ($) of shiftable load scheme for bus *sh*
$Cost^{cur}_{cu,\psi,t}$ load control cost ($) of curtailable load scheme for bus *cu*
$Cost^{tra}_{tr,\psi,t}$ load control cost ($) of transferable load scheme for bus *tr*
$VOLL^{shed}_{i,\psi,t}$ value of lost load ($) for load *i*

Line & bus

$\alpha_{i,m}$ binary variable: 1 if bus *i* belongs to microgrid *m*: 0 otherwise.
λ_i binary variable: 1 if bus *i* is the main bus: 0 otherwise.
β_l binary variable: 1 if line *l* is active: 0 otherwise.
$\beta_{l,m}$ binary variable: 1 if line *l* in microgrid *m* is active: 0 otherwise.
$\beta^{pos}_{l,m,t}, \beta^{neg}_{l,m,t}$ auxiliary variables indicating the status of line *l* in microgrid *m* at time *t*
$F^{flow}_{l,m,\psi,t}$ auxiliary variable indicating fictitious power flow of line *l* in microgrid *m*
PL_l binary variable: 1 if line *l* is functional: 0 otherwise.
PB_i binary variable: 1 if bus *i* is functional: 0 otherwise.
$P^{load}_{i,m,\psi,t}, Q^{load}_{i,m,\psi,t}$ active (kW) and reactive (kVar) power of load *i* in microgrid *m*
$P^{flow}_{l,m,\psi,t}, Q^{flow}_{l,m,\psi,t}$ active (kW) and reactive (kVar) power flow of line *l* in microgrid *m*
$P^{inj}_{i,m,\psi,t}, Q^{inj}_{i,m,\psi,t}$ active (kW) and reactive (kVar) power injection to bus *i* in microgrid *m*
$P^{flow,pos}_{l,m,\psi,t}, P^{flow,neg}_{l,m,\psi,t}$ auxiliary variables indicating the power flow status of line *l* in microgrid *m*
$V_{i,m,\psi,t}$ voltage magnitude of bus *i* in microgrid *m*
$\theta_{i,m,\psi,t}$ voltage angle of bus *i* in microgrid *m*
$P^{source}_{m,\psi,t}$ auxiliary variable for Point of common coupling (PCC) power injection

Resiliency Indices

$Res^{MG}_{m,\psi}$ microgrid resilience index
Res^{Net}_{ψ} network resilience index

medium to large size power systems. In Xu et al. (2016), a resiliency-based methodology was presented to use MGs for restoring critical loads after a major disturbance. This work considers the stability of MGs and technical bounds on the transient current and voltage of DGs as well as frequency deviation as constraints of the load restoration problem. In Zadsar et al. (2017), a metaheuristics algorithm was proposed to optimally operate the smart distribution network considering MG formation in the presence of distributed energy resources. The authors neglected different demand response programs for the optimal operation of the distribution system. In Zhu et al. (2020), a MG formation model was proposed considering voltage and power loss constraints in the operation and power balance feasibility. The model considers exact power flow equations tackled by a mixed-integer linear programming (MILP). In Biswas et al. (2021), a chance-constrained optimal distribution network partitioning was proposed for identifying the best candidates for microgrid formation after HR event.

On the other hand, various types of control strategies can be deployed for DGs that may result in different operation schemes for system restoration. For example, droop-control method was widely used as a control strategy for DGs. Droop-based methods do not need communication among DGs. However, current circulation among DGs is recognized as a main drawback of droop control method. Therefore, the master-slave control concept was utilized to solve the mentioned problem. In this concept, one DG unit can control the voltage and frequency of the distribution system, which is stated as the master unit. The rest of DG units are stated as the slave units that work in current control mode. Thus, the master-slave control technique (Alizadeh et al., 2020; Gilani et al., 2020; Momen et al., 2021, 2020) is frequently used for MG formation problem in distribution system resilience studies. In Alizadeh et al. (2020), a bi-level optimization model based on master-slave technique (MST) was presented to boost the distribution system resilience after natural disasters considering the availability of fast-charging stations. In the lower level, the dynamic charging demand of in-service stations is determined according to the transportation network constraints and the upper level determines the boundaries of the islands for maximizing the recovered loads. In Gilani et al. (2020), an MILP model was presented to recover critical loads based on MG formation and optimal management of distributed energy resources after extreme events. In Momen et al. (2021), a two-stage optimization was proposed for enhancing the resilience of distribution systems after an HR event using distributed energy resources. A single-objective model was introduced in (Momen et al., 2020) to form MGs by means of electric vehicles and direct load control to restore critical loads. The proposed model in this work reduces the number of binary and continuous variables leading to significant enhancement in computational performance of the problem. A method was presented in Sedzro et al. (2017) to optimally form MGs aiming at recovering critical loads after a disturbance. However, these works did not consider various demand response programs including transferable, curtailable, and shiftable loads to improve distribution system resilience in extreme conditions. In addition, load restoration is just considered as a single-objective optimization in these works.

Implementing demand response programs is an effective measure for improving the resilience of distribution systems against HR events. Critical loads could be restored more efficiently as non-critical loads are shed or shifted according to contracts between customers and distribution system operator (DSO). In Shi et al. (2021), a post-event restoration model was presented to enhance distribution system resilience by considering distributed energy resources. This work considers critical loads and interruptible loads as a demand response program to enhance the resilience of distribution systems after HR events. In Bynum et al. (2019), a grid-centric stochastic programming model was proposed to employ demand response for enhancing network resilience instead of investing in transmission line hardening. However, this work considered

Table 1
Survey of previous resilience studies.

Reference	Test system		Formulation	Power Flow	Solving method		Uncertainty modeling			OF		Operational strategies		
	Transmission	Distribution			Mathematical	Heuristic	Load	PV	WT	Load restoration	Operation cost	Reconfiguration	MG formation using MSC	Demand response programs
(Sedzro et al., 2018)		✓	Heuristic	Linearized DistFlow		✓				✓				
(Zadsar et al., 2017)		✓	Heuristic	AC power flow		✓					✓	✓		✓
(Zhu et al., 2020)		✓	MINLP	Modified DistFlow	✓					✓		✓		
(Biswas et al., 2021)		✓	MILP	Linearized Distribution Flow	✓		✓	✓	✓	✓		✓		
(Alizadeh et al., 2020)		✓	MILP	Linearized power flow	✓				✓	✓		✓	✓	✓
(Gilani et al., 2020)		✓	MILP	Linearized power flow	✓		✓	✓	✓	✓		✓	✓	✓
(Momen et al., 2020)		✓	MILP	Linearized DistFlow	✓		✓			✓	✓	✓	✓	✓
(Shi et al., 2021)		✓	MILP	Linearized DistFlow	✓			✓			✓	✓		✓
(Bynum et al., 2019)	✓		MINLP	DC power flow	✓									✓
(Hafiz et al., 2019)		✓	MILP	AC power flow	✓		✓	✓		✓				✓
Current work		✓	MILP	Linearized power flow	✓		✓	✓	✓	✓	✓	✓	✓	✓

demand response contracts for chemical process facilities in transmission network. In Hafiz et al. (2019), a framework for resilient distribution service restoration was presented by considering the integrated control of household flexible appliances to shape the demand curve. This work did not use dynamic MG formation to restore critical loads after HR events. Also, restoration cost is not considered as an objective function for implementing demand response programs. The classification of previous resilience studies is summarized in Table 1 which includes test system, formulation, power flow (PF), solving method, uncertainty modeling, objective functions (OF), and operational strategies.

Thus, in the above discussions, none of the articles considered a joint scheme of dynamic MG formation along with different demand response programs as operational strategies in the service restoration process. In addition, there is a gap in recent studies for a mathematical formulation addressing the multi-objective optimization of load recovery and operation costs in the post-event service restoration process. Therefore, in this paper, a cost-restoration stochastic optimization is introduced as an MILP model in order to fill the gaps of previous research studies. The key contributions of the proposed approach are the following:

- A novel two-objective stochastic optimization model is proposed to maximize the network load restoration and minimize operation costs considering the uncertainties of load, wind speed, and solar radiation. The proposed model examines efficient operation of MGs under real conditions after HR events.
- The ε-constraint method is used to solve the two-objective model and the fuzzy satisfying technique is deployed to choose the best possible solution.
- MG formation and demand response programs including transferable, curtailable, and shiftable loads are employed for enhancing the distribution system resilience.

The remainder of this paper is organized as follows. The two-objective optimization model is formulated in Section 2 incorporating MG formation and demand response programs. The ε-constraint method and fuzzy-based technique for compromising the optimal solution are discussed in Section 3. Numerical studies are presented in Section 4. Finally, the conclusive remarks are drawn in Section 5.

2. Problem formulation

Fig. 1 shows the flowchart of the post-event restoration model for distribution networks against HR events. As damaged lines and buses are determined in Stage 1, the schedulable area for microgrid formation is identified in Stage 2. Schedulable area is the set of nodes and lines not connected to the upstream network. In the presented model, the electricity distribution network is divided into several MGs using distributed generators and automatic switches to minimize the load not supplied and operation costs. Therefore, a multi-objective restoration model is proposed in Stage 3 considering MG formation and operation constraints as well as smart grid technologies. Resilience indices are then calculated to assess the distribution network performance in the restoration process. Detailed formulation of the objective functions and associated constraints of Stage 3 are presented in the following.

2.1. Topological constraints

Graph theory algorithm is an applicable technique to consider MG formation topological constraints (Ding et al., 2017; Mousavizadeh et al., 2018). In the presented model, a network graph involving all the lines and nodes is extracted. Since tie lines are considered, the network graph will contain several loops. In addition, at least one DG with the ability to control the bus voltages and frequency in each MG is required which is called the master unit. In case of multiple DGs in a MG, only one of them will be chosen as the master unit and the others will be

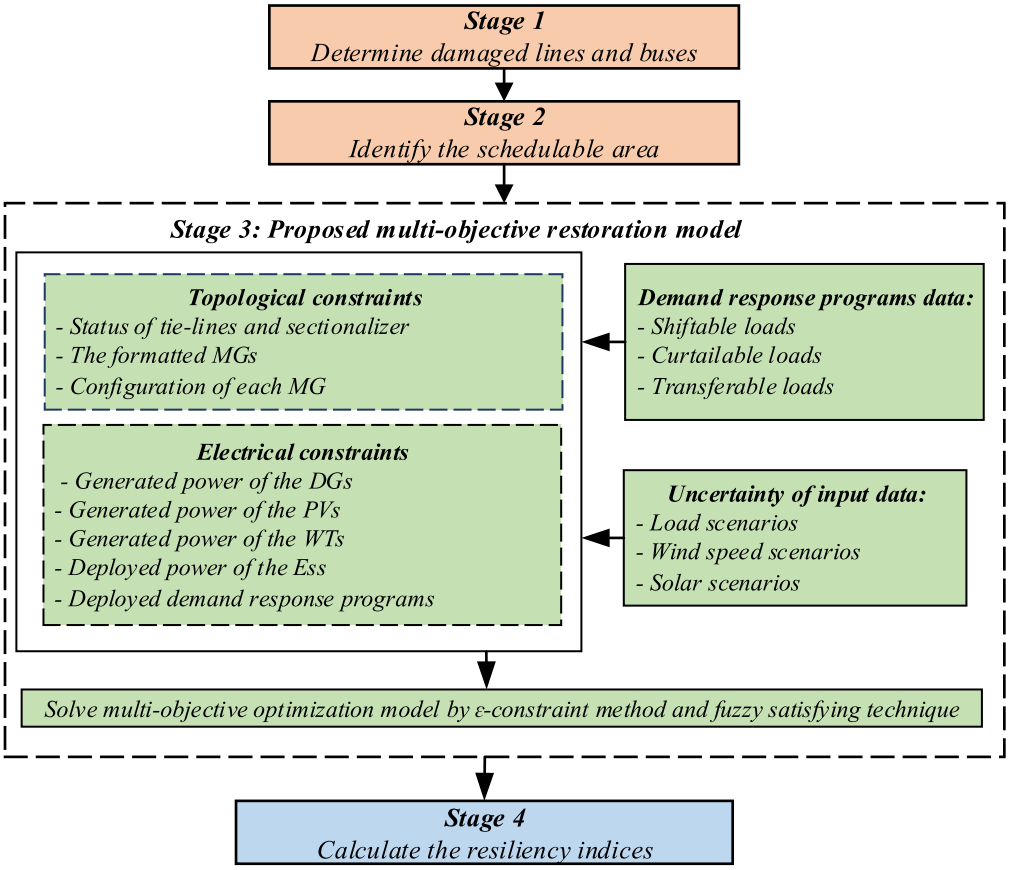

Fig. 1. The flowchart of the proposed two-objective restoration model.

considered as slave units. More explanations about the master-slave control technique are given in (Ding et al., 2017). Thus, the topological constraints are formulated as follows.

$$\sum_{m=1}^{N^{mdg}} \alpha_{i,m} \le 1, \forall i \tag{1}$$

$$\alpha_{i,m} \le \alpha_{r,m}, \forall i, m, r \in i^{MDG} \tag{2}$$

$$\beta_l = \sum_{m=1}^{N^{mdg}} \beta_{l,m}, \forall l \tag{3}$$

$$\beta_{l,m} \le \alpha_{i,m}, i = i^{From}(l), \forall l, m \tag{4}$$

$$\beta_{l,m} \le \alpha_{i,m}, i = i^{To}(l), \forall l, m \tag{5}$$

$$\beta_{l,m} \ge \alpha_{i,m} + \alpha_{r,m} - 1, i = i^{From}(l), r = i^{To}(l), \forall l, m \tag{6}$$

$$\beta_l \le PL_l, \forall l \tag{7}$$

$$\alpha_{i,m} \le PB_i, \forall i, \forall m \tag{8}$$

$$\alpha_{i,m} = \alpha_{r,m}, i = i^{From}(l), r = i^{To}(l), \forall m, l \in L^{nots} \tag{9}$$

$$\sum_{l=1}^{N^L} \left[Sign_{i,l,\psi} \times F^{flow}_{l,m,\psi,t} \right] = P^{inj}_{i,m,\psi,t}, \forall i, \psi, m, t \tag{10}$$

$$\lambda_i P^{source}_{m,\psi,t} + P^{inj}_{i,m,\psi,t} = P^{load}_{i,m,\psi,t}, \forall i, \psi, m, t \tag{11}$$

$$P^{flow,pos}_{l,m,\psi,t} \le P^{flow,\max}_{l} \times \beta^{pos}_{l,m,\psi,t}, \forall l, \psi, m, t \tag{12}$$

$$P^{flow,neg}_{l,m,\psi,t} \le P^{flow,\max}_{l} \times \beta^{neg}_{l,m,\psi,t}, \forall l, \psi, m, t \tag{13}$$

$$F^{flow}_{l,m,\psi,t} = P^{flow,pos}_{l,m,\psi,t} - P^{flow,neg}_{l,m,\psi,t}, \forall l, \psi, m, t \tag{14}$$

$$\beta^{pos}_{l,m,\psi,t} + \beta^{neg}_{l,m,\psi,t} \le \beta_{l,m}, \forall l, \psi, m, t \tag{15}$$

$$\sum_{m=1}^{N^{mdg}} \sum_{l=1}^{N^L} \left[\beta^{pos}_{l,m,\psi,t} - \beta^{neg}_{l,m,\psi,t} \right] \times Sign_{i,l,\psi} \le 1, \forall i, \psi, t \tag{16}$$

In this model, each node will only belong to one MG or it will not belong to any MGs as imposed in Eq. (1). Eq. (2) models the root node constraint. Node i can be connected to MG m if the m^{th} member of i^{MDG} is selected as the root node. Constraints (3)-(6) indicate that if the buses on two sides of a line are not located on the same MG, the binary variable status of the line is set to zero. Eqs. (7) and (8) denote the line status and the failure state of the damaged buses. Installing remote control switches on all lines in an electrical distribution network is not economically feasible. Hence, constraint (9) indicates the switch status on the distribution lines. A spanning tree search technique (Mousavizadeh et al., 2018) is employed to eliminate unconnected loops and nodes to ensure radiality in each MG. The radiality model is formulated by constraints (10)-(16).

2.2. Electrical constraints

2.2.1. Load flow constraints

In this paper, the method presented in Yuan et al., 2016) is utilized to perform load flow computations in the distribution network. Using this approach, the node voltage magnitudes and angles are computed according to a linear approximation. Linearized power flow equations in

electrical distribution networks can be expressed by Eqs. (17)–(20). Eqs. (17) and (18) represent the power balance constraints in each bus. In addition, Eqs. (19) and (20) represent the power flow constraints of distribution lines. Also, the limitations of the slack variables are defined in Eqs. (21)–(27).

$$\sum_{m=1}^{N^{mdg}}\left(P^{DG}_{i,m,\psi,t}+P^{sor}_{i,m,\psi,t}+P^{wnd}_{i,m,\psi,t}+P^{ES,dch}_{i,m,\psi,t}-P^{ES,ch}_{i,m,\psi,t}-P^{load}_{i,m,\psi,t}\right) = -\sum_{m=1}^{N^{mdg}}P^{inj}_{i,m,\psi,t},\forall i,\psi,m,t \tag{17}$$

$$\sum_{m=1}^{N^{mdg}}\left(Q^{DG}_{i,m,\psi,t}-Q^{load}_{i,m,\psi,t}\right) = -\sum_{m=1}^{N^{mdg}}Q^{inj}_{i,m,\psi,t},\forall i,\psi,t \tag{18}$$

$$-\beta_{l,m}\times P^{flow,\max}_{l}\le P^{flow}_{l,m,\psi,t}\le \beta_{l,m}\times P^{flow,\max}_{l},\forall l,m,\psi,t \tag{19}$$

$$-\beta_{l,m}\times Q^{flow,\max}_{l}\le Q^{flow}_{l,m,\psi,t}\le \beta_{l,m}\times Q^{flow,\max}_{l},\forall l,m,\psi,t \tag{20}$$

$$\sum_{m=1}^{N^{mdg}}\left[P^{flow}_{l,m,\psi,t}-BigM\times\left(1-\beta_{l,m}\right)\right]\le\sum_{i\in i^{From}}\sum_{r\in i^{To}}\left[\left[V_{i,m,\psi,t}-V_{r,m,\psi,t}\right]\times Z1^{l}+\left[\theta_{i,m,\psi,t}-\theta_{r,m,\psi,t}\right]\times Z2^{l}\right],\forall l,m,\psi \tag{21}$$

$$\sum_{m=1}^{N^{mdg}}\left[P^{flow}_{l,m,\psi,t}-BigM\times\left(1-\beta_{l,m}\right)\right]\ge\sum_{i\in i^{From}}\sum_{r\in i^{To}}\left[\left[V_{i,m,\psi,t}-V_{r,m,\psi,t}\right]\times Z1^{l}+\left[\theta_{i,m,\psi,t}-\theta_{r,m,\psi,t}\right]\times Z2^{l}\right],\forall l,m,\psi \tag{22}$$

$$\sum_{m=1}^{N^{mdg}}\left[Q^{flow}_{l,m,\psi,t}-BigM\times\left(1-\beta_{l,m}\right)\right]\le\sum_{i\in i^{From}}\sum_{r\in i^{To}}\left[\left[V_{i,m,\psi,t}-V_{r,m,\psi,t}\right]\times Z2^{l}+\left[\theta_{i,m,\psi,t}-\theta_{r,m,\psi,t}\right]\times Z1^{l}\right],\forall l,m,\psi \tag{23}$$

$$\sum_{m=1}^{N^{mdg}}\left[Q^{flow}_{l,m,\psi,t}-BigM\times\left(1-\beta_{l,m}\right)\right]\ge\sum_{i\in i^{From}}\sum_{r\in i^{To}}\left[\left[V_{i,m,\psi,t}-V_{r,m,\psi,t}\right]\times Z2^{l}+\left[\theta_{i,m,\psi,t}-\theta_{r,m,\psi,t}\right]\times Z1^{l}\right],\forall l,m,\psi \tag{24}$$

$$0.9\le V_{i,m,\psi,t}\le 1.1,\forall i,\psi,m,t \tag{25}$$

$$-\left(1-\alpha_{i,m}\right)\times\theta^{\max}\le\theta_{i,m,\psi,t}\le\left(1-\alpha_{i,m}\right)\times\theta^{\max},\forall\psi,m,t,i=i^{MDG}(m) \tag{26}$$

$$-\alpha_{i,m}\times\theta^{\max}\le\theta_{i,m,\psi,t}\le\alpha_{i,m}\times\theta^{\max},\forall i,\psi,m,t \tag{27}$$

2.2.2. Demand response constraints

2.2.2.1. Shiftable loads. Shiftable demand response does not restrict power consumption at each time slot as long as it is able to satisfy the total load demand within a pre-specified time interval Song et al., 2020). The shiftable load constraints are presented in Eqs. (28)–(32). Eq. (28) indicates the net power transferred on the bus for shiftable load unit *sh*. Eq. (29) denotes that the sum of increased power transfer should not exceed the decreased power transfer for each load unit *sh* during the demand response contracts. Constraints (30) and (31) restrict the increased and decreased power transfers to their maximum allowed values for each load unit *sh*, respectively. Constraint (32) enforces that the power transfer for load unit *sh* cannot be increased or decreased at the same time.

$$\sum_{m=1}^{N^{mdg}}P^{sha}_{sh,m,\psi,t}=P^{sha,up}_{sh,\psi,t}-P^{sha,down}_{sh,\psi,t},\forall sh,\psi,t \tag{28}$$

$$\sum_{t}P^{sha,up}_{sh,\psi,t}-\sum_{t}P^{sha,down}_{sh,\psi,t}\le 0,\forall sh,\psi \tag{29}$$

$$P^{sha,up}_{sh,\psi,t}\le\delta^{sha,up}_{sh,\psi,t}\times LPF^{sha,up}\times P^{load,pre}_{i,\psi,t},\forall\psi,t,i\in sh \tag{30}$$

$$P^{sha,down}_{sh,\psi,t}\le\delta^{sha,down}_{sh,\psi,t}\times LPF^{sha,down}\times P^{load,pre}_{i,\psi,t},\forall\psi,t,i\in sh \tag{31}$$

$$\delta^{sha,up}_{sh,\psi,t}+\delta^{sha,down}_{sh,\psi,t}\le 1,\forall sh,\psi,t \tag{32}$$

2.2.2.2. Curtailable loads

Curtailable demand response allows power curtailment within a specific period while it may cause the load to rebound in the subsequent hours Song et al., 2020). The curtailable load constraints are shown in Eqs. (33)–(37). Constraint (33) indicates the net power transferred on the bus for curtailable load unit *cu*. Constraint (34) denotes that the sum of decreased and increased power transfers should be zero during the demand response contracts for each load unit *cu*. It could be implied that the increased power transfer in time *t* should be formerly decreased during three hours based on the predetermined coefficients. Eqs. (35) and (36) restrict the increased and decreased power transfers to their maximum allowed values for each load unit *cu*, respectively. Eq. (37) indicates that the power transfer for load unit *cu* cannot be increased or decreased at the same time.

$$\sum_{m=1}^{N^{mdg}}P^{cur}_{cu,m,\psi,t}=P^{cur,up}_{cu,\psi,t}-P^{cur,down}_{cu,\psi,t},\forall cu,\psi,t \tag{33}$$

$$P^{cur,up}_{cu,\psi,t}=0.6\times P^{cur,down}_{cu,\psi,t-1}+0.3\times P^{cur,down}_{cu,\psi,t-2}+0.1\times P^{cur,down}_{cu,\psi,t-3},\forall cu,\psi,t \tag{34}$$

$$P^{cur,up}_{cu,\psi,t}\le\delta^{cur,up}_{cu,\psi,t}\times LPF^{cur,up}\times P^{load,pre}_{i,\psi,t},\forall\psi,t,i\in cu \tag{35}$$

$$P^{cur,down}_{cu,\psi,t}\le\delta^{cur,down}_{cu,\psi,t}\times LPF^{cur,down}\times P^{load,pre}_{i,\psi,t},\forall\psi,t,i\in cu \tag{36}$$

$$\delta^{cur,up}_{cu,\psi,t}+\delta^{cur,down}_{cu,\psi,t}\le 1,\forall cur,\psi,t \tag{37}$$

2.2.2.3. Transferable loads. Transferable demand response provides the loads with a flexibility in transferring the starting time while the consumption duration is fixed. Once started, the transferable load cannot be interrupted and hence the daily load remains constant Song et al., 2020). This concept is modeled by Eqs. (38)–(42). Eq. (38) denotes the net power transferred on the bus for transferrable load unit *tr*. Eq. (39) indicates that the sum of decreased and increased power transfers should be zero for each load unit *tr* during the demand response contracts. It is worth mentioning that the decreased power transfer in time *t* should be formerly compensated by an increased power transfer in *t*-τ. Constraints (40) and (41) limit the increased and decreased power transfers to their maximum allowed values for each load unit *tr*, respectively. Constraint (42) denotes that the power transfer for load unit *tr* cannot be increased or decreased at the same time.

$$\sum_{m=1}^{N^{mdg}}P^{tra}_{tr,m,\psi,t}=P^{tra,up}_{tr,\psi,t}-P^{tra,down}_{tr,\psi,t},\forall tr,\psi,t \tag{38}$$

$$P^{tra,up}_{tr,\psi,t-\tau}-P^{tra,down}_{tr,\psi,t}=0,\forall tr,\psi,t \tag{39}$$

$$P^{tra,up}_{tr,\psi,t}\le\delta^{tra,up}_{tr,\psi,t}\times LPF^{tra,up}\times P^{load,pre}_{i,\psi,t},\forall\psi,t,i\in tr \tag{40}$$

$$P^{tra,down}_{tr,\psi,t}\le\delta^{tra,down}_{tr,\psi,t}\times LPF^{tra,down}\times P^{load,pre}_{i,\psi,t},\forall\psi,t,i\in tr \tag{41}$$

$$\delta^{tra,up}_{tr,\psi,t}+\delta^{tra,down}_{tr,\psi,t}\le 1,\forall tr,\psi,t \tag{42}$$

2.2.3. Load constraints

Eqs. (43)–(52) indicate the active and reactive load constraints with regards to the demand response programs.

$$P^{load}_{i,m,\psi,t}=\alpha_{i,m}\times P^{load,pre}_{i,\psi,t}+P^{sha}_{sh,m,\psi,t},\forall\psi,m,t,i\in sh \tag{43}$$

$$P^{load}_{i,m,\psi,t} = \alpha_{i,m} \times P^{load,pre}_{i,\psi,t} + P^{cur}_{cu,m,\psi,t}, \forall \psi, m, t, i \in cu \quad (44)$$

$$P^{load}_{i,m,\psi,t} = \alpha_{i,m} \times P^{load,pre}_{i,\psi,t} + P^{tra}_{tr,m,\psi,t}, \forall \psi, m, t, i \in tr \quad (45)$$

$$P^{load}_{i,m,\psi,t} = \alpha_{i,m} \times P^{load,pre}_{i,\psi,t} - P^{shed}_{i,m,\psi,t}, \forall \psi, m, t, i \in q \quad (46)$$

$$P^{load}_{i,m,\psi,t} \le \alpha_{i,m} \times BigM, \forall \psi, m, t, i \in j \quad (47)$$

$$Q^{load}_{i,m,\psi,t} = \alpha_{i,m} \times Q^{load,pre}_{i,\psi,t} + \tan(\phi_{i,\psi}) \times P^{sha}_{i,m,\psi,t}, \forall \psi, m, t, i \in sh \quad (48)$$

$$Q^{load}_{i,m,\psi,t} = \alpha_{i,m} \times Q^{load,pre}_{i,\psi,t} + \tan(\phi_{i,\psi}) \times P^{cur}_{i,m,\psi,t}, \forall \psi, m, t, i \in cu \quad (49)$$

$$Q^{load}_{i,m,\psi,t} = \alpha_{i,m} \times Q^{load,tra}_{i,\psi,t} + \tan(\phi_{i,\psi}) \times P^{tra}_{i,m,\psi,t}, \forall \psi, m, t, i \in tr \quad (50)$$

$$Q^{load}_{i,m,\psi,t} = \alpha_{i,m} \times Q^{load,pre}_{i,\psi,t} - \tan(\phi_{i,\psi}) \times P^{shed}_{i,m,\psi,t}, \forall \psi, m, t, i \in q \quad (51)$$

$$Q^{load}_{i,m,\psi,t} \le \alpha_{i,m} \times BigN, \forall \psi, m, t, i \in j \quad (52)$$

2.2.4. Constraints of DGs and energy storage units

2.2.4.1. DGs. Technical constraints of DGs for active and reactive power generation are shown in Eqs. (53) and (54).

$$\alpha_{i,m} \times P^{DG,\min}_{dg} \le P^{DG}_{dg,m,\psi,t} \le \alpha_{i,m} \times P^{DG,\max}_{dg}, i = i^{DG}(dg), \forall dg, \psi, m, t \quad (53)$$

$$\alpha_{i,m} \times Q^{DG,\min}_{dg} \le Q^{DG}_{dg,m,\psi,t} \le \alpha_{i,m} \times Q^{DG,\max}_{dg}, i = i^{DG}(dg), \forall dg, \psi, m, t \quad (54)$$

2.2.4.2. PVs

Eq. (55) represents the output power constraint of PV units:

$$P^{sor}_{pv,m,\psi,t} \le \alpha_{i,m} \times P^{sor,\max}_{pv,\psi,t}, i = i^{sor}(pv), \forall pv, \psi, m, t \quad (55)$$

2.2.4.3. Wind turbines. Eq. (56) formulates the output power constraints of the wind turbines:

$$P^{wnd}_{w,m,\psi,t} \le \alpha_{i,m} \times P^{wnd,\max}_{w,\psi,t}, i = i^{wnd}(w), \forall w, \psi, m, t \quad (56)$$

2.2.4.4. Energy storage units. Eqs. (57)–(60) show the charging and discharging constraints of the energy storage units. In addition, Eqs. (61)–(63) show maximum, minimum, and initial charge level constraints of energy storage units, respectively. The mathematic calculation of SOC is denoted in Eq. (64).

$$\gamma^{ES}_{e,m,\psi,t} \le \alpha_{i,m}, i = i^{ES}(e), \forall e, \psi, m, t \quad (57)$$

$$P^{ES,ch}_{e,m,\psi,t} \le \gamma^{ES}_{e,m,\psi,t} \times RT^{ch,\max}_{e}, \forall e, \psi, m, t \quad (58)$$

$$P^{ES,dch}_{e,m,\psi,t} \le \left(1 - \gamma^{ES}_{e,m,\psi,t}\right) \times RT^{dch,\max}_{e}, \forall e, \psi, m, t \quad (59)$$

$$P^{ES,dch}_{e,m,\psi,t} \le \alpha_{i,m} \times RT^{dch,\max}_{e}, i = i^{ES}(e), \forall e, \psi, m, t \quad (60)$$

$$P^{SOC}_{e,m,\psi,t} \le \alpha_{i,m} \times SOC^{max}_{e}, i = i^{ES}(e), \forall e, \psi, m, t \quad (61)$$

$$P^{SOC}_{e,m,\psi,t} \ge \alpha_{i,m} \times SOC^{\min}_{e}, i = i^{ES}(e), \forall e, \psi, m, t \quad (62)$$

$$P^{SOC}_{e,m,\psi,t} = \alpha_{i,m} \times SOC^{initial}_{e} + P^{ES,ch}_{e,m,\psi,t} \times \eta^{ES}_{e} - P^{ES,dch}_{e,m,\psi,t} \times \frac{1}{\eta^{ES}_{e}}, i = i^{ES}(e), t = 1, \forall e, \psi, m \quad (63)$$

$$P^{SOC}_{e,m,\psi,t} = P^{SOC}_{e,m,\psi,t-1} + P^{ES,ch}_{e,m,\psi,t} \times \eta^{ES}_{e} - P^{ES,dch}_{e,m,\psi,t} \times \frac{1}{\eta^{ES}_{e}}, t > 1, \forall e, \psi, m \quad (64)$$

2.2.5. Bus voltage constraints

Eqs. (65) and (66) show the bus voltage magnitude and angle constraints, respectively. Moreover, Eq. (67) indicates that if DG m is chosen as the master unit, the voltage of the corresponding bus is set to the desired value. In addition, the voltage angle of the corresponding bus is set to zero by Eq. (68).

$$\gamma_{i,k} \times V^{Min} \le V_{i,k,t,\omega} \le \gamma_{i,k} \times V^{Max}, \forall i \in B, \forall k \in K, \forall t \in T, \forall \omega \in \Omega \quad (65)$$

$$-\gamma_{i,k} \times \delta^{Max} \le \delta_{i,k,t,\omega} \le \gamma_{i,k} \times \delta^{Max}, \forall i \in B, \forall k \in K, \forall t \in T, \forall \omega \in \Omega \quad (66)$$

$$V_{i,k,t,\omega} = \gamma_{i,k} \times V^{DG,set}_{k}, \forall i \in B_{MDG}, \forall k \in K, \forall t \in T, \forall \omega \in \Omega \quad (67)$$

$$-\left(1 - \gamma_{i,k}\right) \times \delta^{Max} \le \delta_{i,k,t,\omega} \le \left(1 - \gamma_{i,k}\right) \times \delta^{Max}, \forall i \in B_{MDG}, \forall k \in K, \forall t \in T, \forall \omega \in \Omega \quad (68)$$

2.2.6. Power balance of MGs

Eq. (69) ensures power balance in each MG.

$$\sum_{g=1}^{N_{DG}} P^{DG,s}_{g,k,t} + \sum_{n=1}^{N_{WT}} P^{WT,s}_{n,k,t} + \sum_{e=1}^{N_{ES}} PES^{dch,s}_{e,k,t} - \sum_{e=1}^{N_{ES}} PES^{ch,s}_{e,k,t} - \sum_{i=1}^{N_{Load}} P^{L,s}_{i,k,t} = 0, \forall k \in K, \forall t \in T \quad (69)$$

2.3. Resilience indices

To assess the performance of the network and MGs, we use the network and MG resilience indices. The network resilience index could be extracted using Eq. (70), which is stated as the ratio of the recovered loads of network to sum of all connected loads to the network considering load priority weights. The MG resilience index is also calculated using Eq. (71), which is expressed as one minus the ratio of the unsupplied loads to the supplied loads in each MG, taking into account the load priority weights.

$$Res^{Net}_{\psi} = \frac{\sum_{i=1}^{N^{bus}} \sum_{m=1}^{N^{mdg}} \sum_{t} F^{pr}_{i,\psi,t} \times P^{load}_{i,m,\psi,t}}{\sum_{i=1}^{N^{bus}} \sum_{t} F^{pr}_{i,\psi,t} \times P^{load,pre}_{i,\psi,t}}, \forall \psi \quad (70)$$

$$Res^{MG}_{m,\psi} = 1 - \frac{\sum_{q} \sum_{t} P^{shed}_{q,m,\psi,t}}{\sum_{i} \sum_{t} P^{load}_{i,m,\psi,t}}, \forall m, \psi \quad (71)$$

2.4. Objective functions

2.4.1. Network load restoration

In the first objective function, the performance of the distribution network against the HR event should be improved. Therefore, the first objective function helps minimize the load not supplied. In other words, the first objective function maximizes the total restored loads of the scenarios based on their priority as shown in Eq. (72):

$$OF_1 = \sum_{\psi} \varepsilon_{\psi} \sum_{i=1}^{N^{bus}} \sum_{t} P^{load,pre}_{i,\psi,t} - \sum_{\psi} \varepsilon_{\psi} \sum_{i=1}^{N^{bus}} \sum_{m=1}^{N^{mdg}} \sum_{t} F^{pr}_{i,\psi,t} \times P^{load}_{i,m,\psi,t} \quad (72)$$

2.4.2. Restoration cost

Restoration cost includes the budget required for implementing demand response programs and power supply from DGs, wind turbines, photovoltaic resources, and energy storage units as written in Eq. (73). The restoration cost should be minimized. Eqs. (74)–(81) detail different elements of restoration cost.

$$OF_2 = \sum_{\psi} \varepsilon_{\psi} \left[\sum_{t} \sum_{sh} Cost^{sha}_{sh,\psi,t} + \sum_{t} \sum_{cu} Cost^{cur}_{cu,\psi,t} + \sum_{t} \sum_{tr} Cost^{tra}_{tr,\psi,t} + \sum_{t} \sum_{q} VOLL^{shed}_{q,\psi,t} + \sum_{t} \sum_{dg} Cost^{DG}_{dg,\psi,t} + \sum_{t} \sum_{pv} Cost^{sor}_{pv,\psi,t} + \sum_{t} \sum_{w} Cost^{wnd}_{w,\psi,t} + \sum_{t} \sum_{e} Cost^{ES}_{e,\psi,t} \right] \tag{73}$$

$$Cost^{sha}_{sh,\psi,t} = \sum_{m=1}^{N^{mdg}} \left[P^{sha,up}_{sh,\psi,t} + P^{sha,down}_{sh,\psi,t} \right] \times \Pr^{sha}_{sh,\psi,t}, \forall sh, \psi, t \tag{74}$$

$$Cost^{cur}_{cu,\psi,t} = \sum_{m=1}^{N^{mdg}} \left[P^{cur,up}_{cu,\psi,t} + P^{cur,down}_{cu,\psi,t} \right] \times \Pr^{cur}_{cu,\psi,t}, \forall cu, \psi, t \tag{75}$$

$$Cost^{tra}_{tr,\psi,t} = \sum_{m=1}^{N^{mdg}} \left[P^{tra,up}_{tr,\psi,t} + P^{tra,down}_{tr,\psi,t} \right] \times \Pr^{tra}_{tr,\psi,t}, \forall tr, \psi, t \tag{76}$$

$$VOLL^{shed}_{q,\psi,t} = \sum_{m=1}^{N^{mdg}} P^{shed}_{i,m,\psi,t} \times \Pr^{shed}_{i,t}, \forall \psi, t \tag{77}$$

$$Cost^{DG}_{dg,\psi,t} = \sum_{m=1}^{N^{mdg}} P^{DG}_{dg,m,\psi,t} \times \Pr^{DG}_{dg,\psi,t}, \forall dg, \psi, t \tag{78}$$

$$Cost^{sor}_{pv,\psi,t} = \sum_{m=1}^{N^{mdg}} P^{sor}_{pv,m,\psi,t} \times \Pr^{sor}_{pv,\psi,t}, \forall pv, \psi, t \tag{79}$$

$$Cost^{wnd}_{w,\psi,t} = \sum_{m=1}^{N^{mdg}} P^{wnd}_{w,m,\psi,t} \times \Pr^{wnd}_{w,\psi,t}, \forall w, \psi, t \tag{80}$$

$$Cost^{ES}_{e,\psi,t} = \sum_{m=1}^{N^{mdg}} \left[P^{ES,ch}_{e,m,\psi,t} + P^{ES,dch}_{e,m,\psi,t} \right] \times \Pr^{ES}_{e,\psi,t}, \forall e, \psi, t \tag{81}$$

2.5. Modeling uncertainty of input data

Most of the models resembling real-world processes have some uncertain parameters. This section uses a scenario-based strategy to model the uncertainty of the network input data, namely the load, wind speed, and solar radiation (Farsangi et al., 2018).

2.5.1. Modeling load uncertainty

The normal probability distribution function is employed to model the load uncertainty as shown in Eq. (82). In this relation, variables μ and δ represent the mean and the standard deviation of the load, respectively (Farsangi et al., 2018).

$$f(x) = \frac{1}{\sigma\sqrt{2\pi}} \exp\left(- \frac{(x-\mu)^2}{2\sigma^2} \right) \tag{82}$$

2.5.2. Modeling the wind speed uncertainty

The Weibull probability density function is used to formulate wind speed prediction errors as shown in Eq. (83). The variables k and c represent the shape and scale indices, respectively, computed by using mean and standard deviation of wind speed (Farsangi et al., 2018).

$$\mathrm{f(v)} = \left(\frac{\mathrm{k}}{\mathrm{c}}\right)\left(\frac{\mathrm{v}}{\mathrm{c}}\right)^{(\mathrm{k}-1)} \exp\left[- \left(\frac{\mathrm{v}}{\mathrm{c}}\right)^{\mathrm{k}} \right] \tag{83}$$

2.5.3. Modeling the solar uncertainty

Beta probability distribution function, shown in Eq. (84), is used to represent the solar radiation uncertainty parameter. The variables α and β are the beta distribution parameters and are calculated according to the mean value and standard deviation of the solar radiation (Farsangi et al., 2018).

$$f(sor) = \begin{cases} \dfrac{\Gamma(\alpha+\beta)}{\Gamma(\alpha)\Gamma(\beta)} \times (sor)^{\alpha-1} \times (1-sor)^{(\beta-1)} 0 \le \mathrm{sor} \le 1, \alpha \ge 0, \beta \ge 0 \\ 0 \text{otherwise} \end{cases} \tag{84}$$

The computational burden of a scenario-based optimization model depends on the number of generated scenarios. Accordingly, it is necessary to reduce the set of main scenarios in such a way that the problem characteristics do not significantly change (Ghasemi et al., 2021). The number of reduced scenarios depends on the nature of the optimization problem. This paper uses the K-means clustering algorithm to reduce the number of scenarios. More details about K-means clustering method are given in (Chévez et al., 2017).

3. Optimization method

The ε-constraint method is utilized to solve the proposed multi-objective optimization model. As the first step in ε-constraint method, the payoff table should be calculated. The payoff table refers to the individual optimization results of the each objective function. After the computation of the payoff table, one of the objective functions is considered as the main function while the other is considered as a constraint for the main objective function (Nojavan et al., 2018). Hence, a single-objective problem can be optimized according to constraint (85).

$$\begin{aligned} &\min\ (OF_1) \\ &\text{s.t.} \\ &\begin{cases} OF_2 \le \varepsilon \\ Equal \text{ and unequal equations} \end{cases} \end{aligned} \tag{85}$$

The single-objective optimization problem is solved for each ε (beginning with $OF_2^{\min}$ and ending with $OF_2^{\max}$), after which optimal solutions are derived. The set of all solutions extracted for all variations of ε are known as the Pareto optimal front of the multi-objective optimization problem. Afterward, the best possible solution is selected from among the obtained solutions by using a fuzzy satisfying technique to convert both of the conflicting objective functions to their respective normalized forms as written in (86) (Amirioun et al., 2018).

$$\mu_k^s = \begin{cases} 1 f_k^s \le f_k^{\min} \\ \dfrac{f_k^{\max} - f_k^s}{f_k^{\max} - f_k^{\min}} f_k^{\min} \le f_k^s \le f_k^{\max} \\ 0 f_k^s \ge f_k^{\max} \end{cases} \tag{86}$$

In the above equation, μ_k^s refers to the membership function of the s^{th} solution of objective function k whereas $f_k^{\min}$ and $f_k^{\max}$ represent minimum and maximum values of the kth objective function in the payoff table, respectively. Then, for each Pareto solution, the minimum membership function is identified:

$$\tau^s = \min\left(\mu_k^s\right), \forall \mathrm{s} \tag{87}$$

Finally, the Pareto solution with the maximum value of τ^s will be selected as the final solution of the multi-objective problem.

From a practical perspective, the Pareto optimal front (POF) helps system operators and managers perceive the status of objective functions at each POF solution in addition to the final solution. In extreme conditions after HR events, managers may prefer to select a non-optimal solution in exchange for satisfying management issues. The decision of managers is biased by different factors including social impacts of load interruptions and economic constraint related to available budget for

Table 2
Required data on generation and storage units.

Unit	Bus	Cap. (kW)	Q_{dg}^{min} (kVAr)	Q_{dg}^{max} (kVAr)	Unit	Bus	Unit	Bus	Unit	Bus
DG1	11	505	−92	92	ES1	20	PV1	24	WT1	18
DG2	25	405	−395	395	ES2	22	PV2	36		
DG3	21	240	−343	343	ES3	35				

Table 3
The characteristics of demand response programs.

DR	Bus	LPF^{up}	LPF^{down}
Curtailable load	3, 14, 15, 17, 18, 19, 26	0.5	0.5
Transferable load	28, 30	0.5	0.5
Shiftable load	32, 33, 34	0.5	0.5

service restoration.

4. Numerical results

In this section, the proposed model is implemented on the IEEE 37-node and the modified 118-node distribution systems. Simulations were performed on a PC with an Intel Core i7–700 2.4 GHz and 8 GB of memory. The proposed model was solved using CPLEX solver under the GAMS environment with a 0.01% relative optimality gap. It is worth mentioning that the proposed microgrid formation-based restoration model can be implemented for the post-event condition after any natural disasters provided that particular consequences of the event such as line outages are accurately accounted for in the model.

4.1. IEEE-37 node distribution network

This test network is configured with one upstream substation, 12 normally-closed lines, and 6 tie lines. The total active and reactive power consumptions of this network are 22.71 MW and 17.04 MVAr, respectively. Detailed information about the system node and line parameters is available in (Borghei & Ghassemi, 2021; Munikoti et al., 2021).

The required information about the location and the capacity of DGs, wind turbines, and energy storage is given in Table 2. In this test network, 2 units (DG1 to DG2) of the 3 existing DGs have the ability to act as a master unit, and hence, the maximum number of formable MGs is equal to 2. The capacity, charging and discharging rates, efficiency, and initial SOC of ES units are assumed to be 50 kWh, 50 kW, 85%, and 60%, respectively. The capacity of wind turbine and photovoltaic units are considered to be 100 and 50 kW, respectively. The associated data on load, wind, and solar power uncertainties has been extracted from Farsangi et al. (2018) and is given in Anon (2022). The characteristics of demand response contracts are presented in Table 3. The operation cost of generation and storage units and demand response programs are shown in Table 4 (Nojavan et al., 2018; Zeynali et al., 2021). Fig. 2

Table 4
The operation cost of generation and storage units and demand response programs.

$Price_{dg,\psi,t}^{DG}$	$Price_{w,\psi,t}^{wnd}$	$Price_{pv,\psi,t}^{sor}$	$Price_{e,\psi,t}^{ES}$	$Price_{sh,\psi,t}^{sha}$	$Price_{tr,\psi,t}^{tra}$	$Price_{cu,\psi,t}^{cur}$	$Price_{q,t}^{shed}$
0.08 $/kWh	0.01 $/kWh	0.01 $/kWh	0.02 $/kWh	0.04 $/kWh	0.02 $/kWh	0.03 $/kWh	100 $/kWh

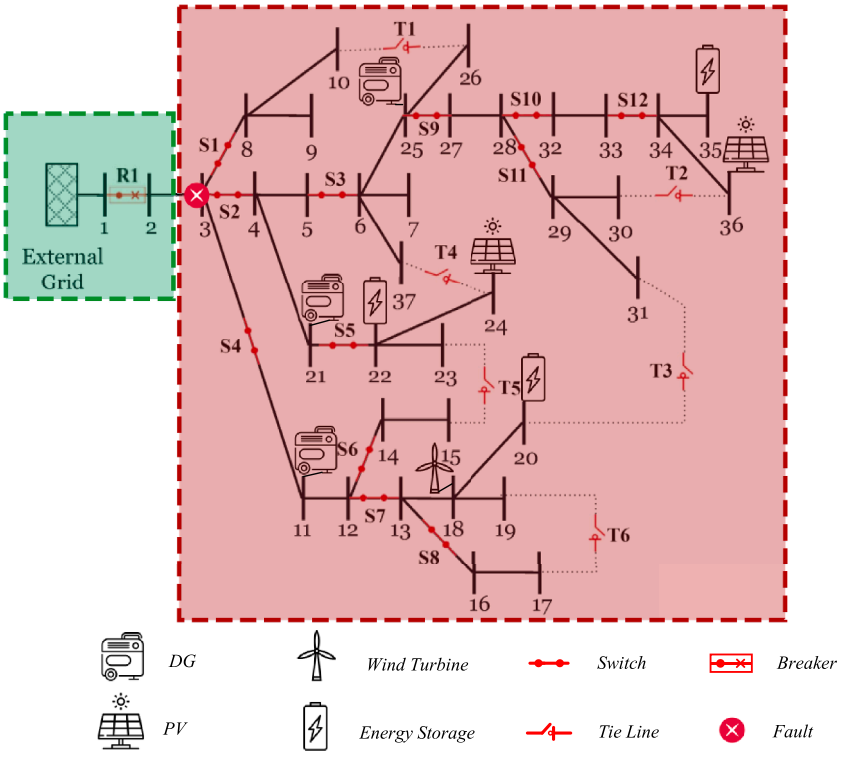

Fig. 2. Single-line diagram of the IEEE 37-bus test network at the event onset.

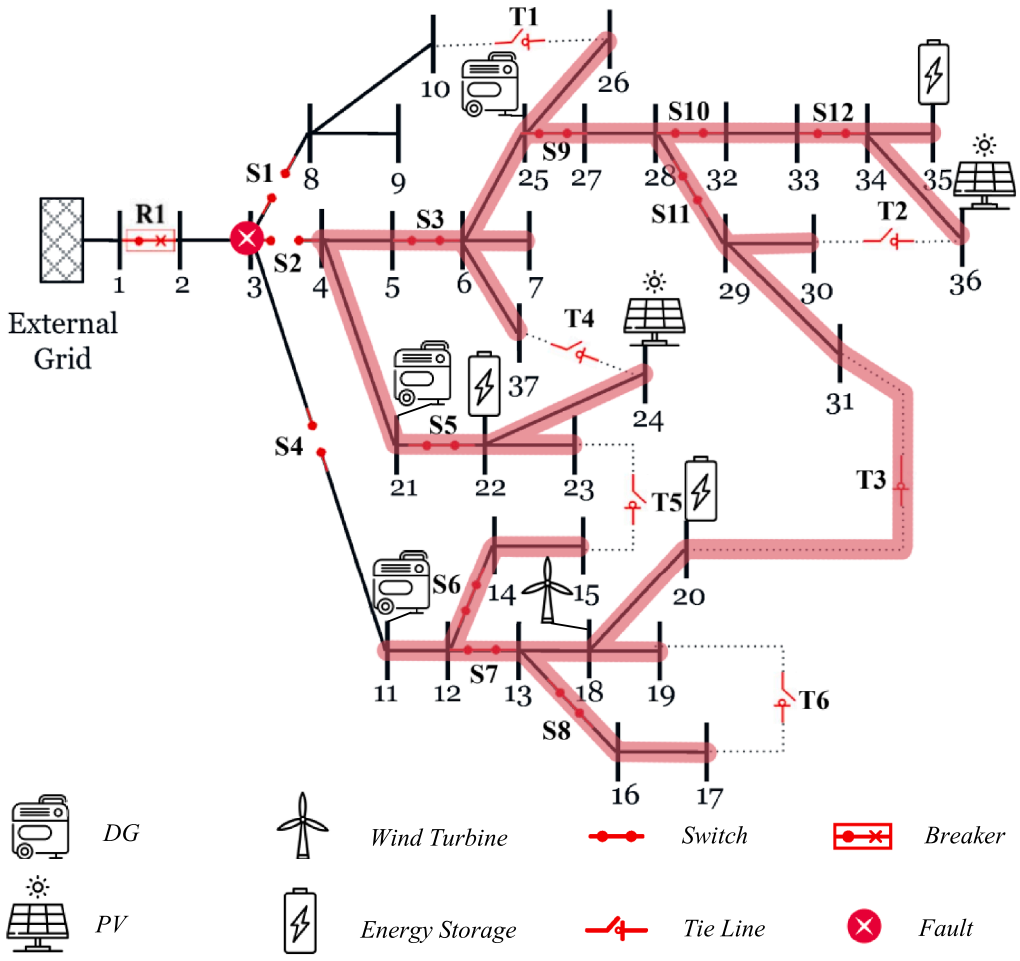

Fig. 3. MG formation in IEEE 37-bus test system in case 1.

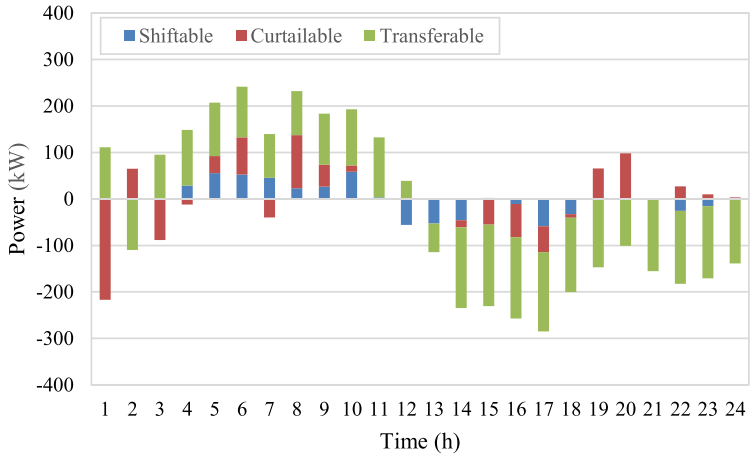

Fig. 4. Different load control schemes during restoration process post the event in case 1.

shows the structure of the IEEE-37 bus network at the event onset. In this paper, it is assumed that the feeder is interrupted from the main substation. Therefore, all nodes after node 3 are in the schedulable area. To explain the effect of utilizing demand response programs and distributed energy resources on the proposed model, two cases are considered as follows:

- Case 1: Single-objective operation based on minimizing load shedding,
- Case 2: Multi-objective operation based on minimizing load shedding and minimizing operation cost.

Table 5
Pay-off table of the ε-constraint method for IEEE 37-bus distribution network in case 2.

Scheduling objective function	Load shedding (kWh)	Restoration cost ($)
Load shedding minimization	4791.66	2428.11
Restoration cost minimization	10,077.16	1812.25

4.1.1. Case 1

In this case, the network scheduling is performed with the sole purpose of supplying the maximum load in the restoration process post the event neglecting the restoration cost. The post-event network structure is shown in Fig. 3. According to this figure, a MG has been formed under the post-event conditions. The supplied energy during the study horizon is 28,511.34 kWh and the operational cost is 2428.11 $. As shown in Fig. 3, the MG formation method has succeeded in using all three DGs in coordination via demand response programs and distributed energy resources. In this case, the network and MG resilience indices are 85.61% and 97.46%, respectively.

Given the three types of demand response schemes, Fig. 4 displays the hourly graph of load control for transferable, curtailable, and shiftable loads. As seen in this figure, a portion of the load at the peak hour is decreased by paying the corresponding cost in each of the 3 load control models. However, they intend to reduce consumption at the load peak by encouraging more consumption at non-peak hours. For example, at 17 o'clock, the shiftable, curtailable and transferable loads are 58.5, 55.9 and 170.8, respectively. Moreover, the value of load reduction in this case is 741.02 kWh. For the sake of brevity, the rest of results on generation profile of DGs and renewable units as well as energy storage scheduling are not presented for case 1.

4.1.2. Case 2

In this case, the scheduling is performed with the aim of minimizing load shedding and the restoration cost. In the first step, the front table is calculated for the two objective functions to compute the normal values. These front values are shown in Table 5. It should be mentioned that these values are obtained from the individual solution of each objective function.

Given the formulation of the main problem and the multi-objective optimization, the epsilon constraint method is used in this study to create the Pareto boundary. In the proposed model, load shedding is chosen as the main objective function and restoration cost is considered as the additional constraint. The number of solution points considered on the Pareto front is 11 and variation steps for the maximum level of the constraint are identical. Numerical results of are summarized in Tables 6 and Fig. 5.

According to Table 6, the minimum membership degree at Point 5 is at its maximum. The restoration cost in this state is 2058.60 $ and the load shedding is 6956.12 kWh. In addition, the network and MG resilience indices are 79.11% and 94.38%, respectively. As predicted, since the restoration cost is used as an additional objective function in this case, the resilience indices are lower than those of case 1. This limitation is near to real behavior of distribution system operators, since the budget for load restoration is not limitless. As shown in Fig. 5, the Pareto solution is the best trade-off between the two objective functions. Given the selected optimal Pareto point, the optimal network structure is shown in Fig. 6.

Table 6
Detailed Pareto solution for IEEE 37-bus distribution network in case 2.

Iteration number	Load shedding (kWh) Load	Restoration cost ($) Cost	Membership degree First objective function (μ_1) mu1	Membership degree Second objective function (μ_2) mu2	Restoration cost limit (epsilon) Limit (Epsilon)	Minimum membership degree min(mu1,mu2)
Iter01	9697.36	1812.25	0.07185	1	1812.2575	0.071857
Iter02	8989.62	1873.84	0.20576	0.9	1873.8437	0.205760
Iter03	8500.40	1930.92	0.29831	0.80732	1935.4299	0.298318
Iter04	7464.79	1997.01	0.49425	0.7	1997.0161	0.494251
Iter05	6956.12	2058.60	0.59049	0.6	2058.6023	0.590491
Iter06	6385.28	2120.18	0.69849	0.5	2120.1885	0.5
Iter07	6062.70	2181.77	0.75952	0.4	2181.7747	0.4
Iter08	5693.88	2243.36	0.82930	0.3	2243.3609	0.3
Iter09	5180.66	2304.94	0.92640	0.2	2304.9470	0.2
Iter10	4866.04	2366.53	0.98592	0.1	2366.5332	0.1
Iter11	4791.66	2425.89	1	0.00360	2428.1194	0.003608

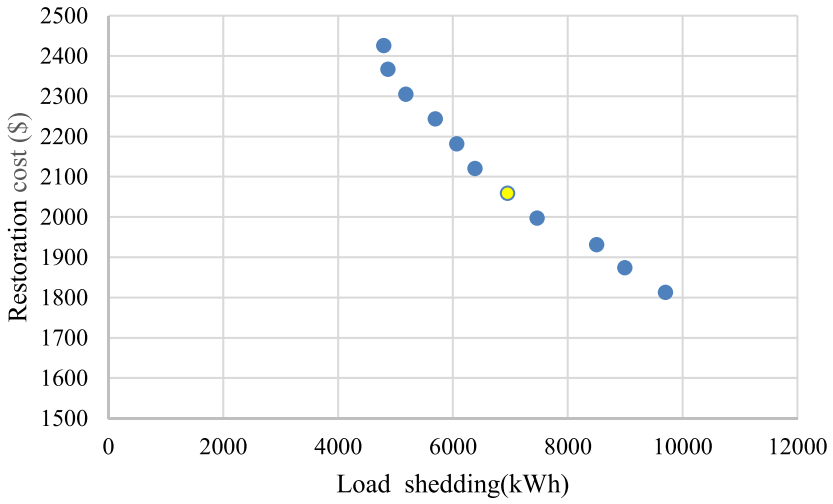

Fig. 5. Pareto-optimal solution for IEEE 37-bus distribution network in case 2.

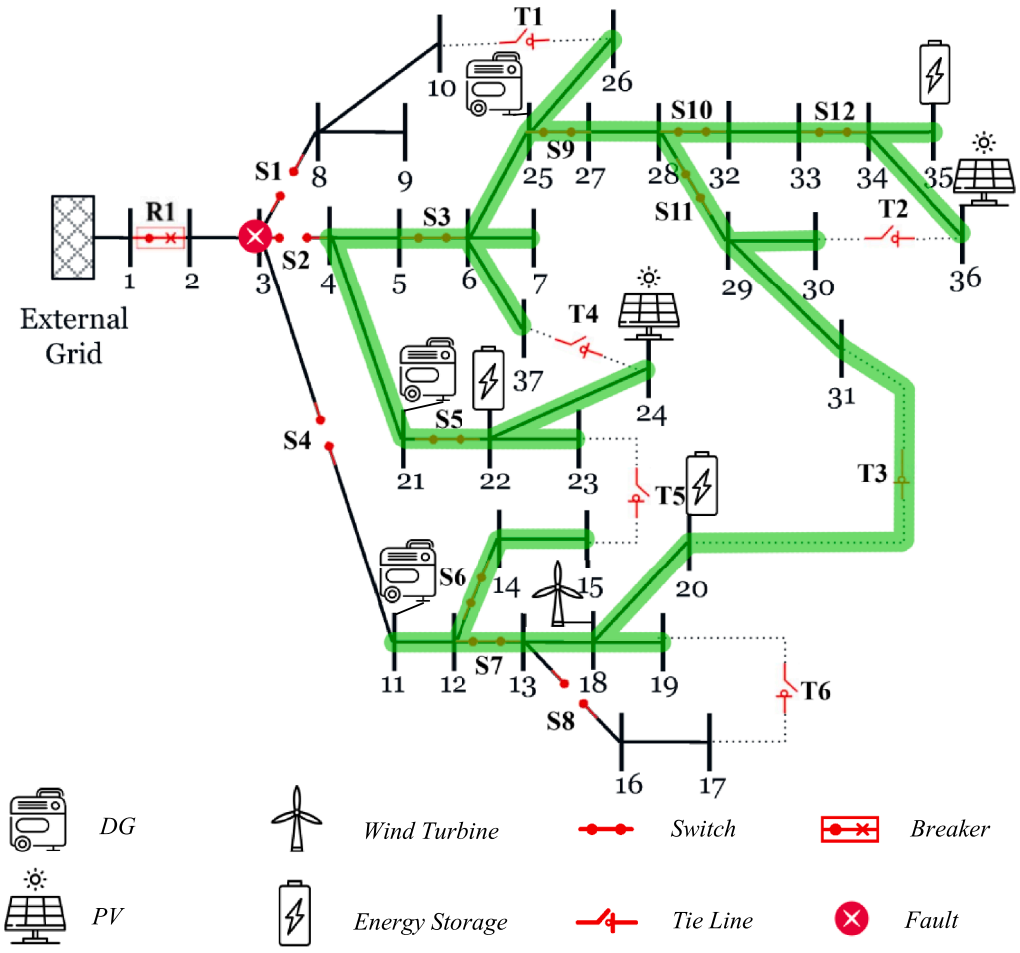

Fig. 6. MG formation in IEEE 37-bus test system in case 2.

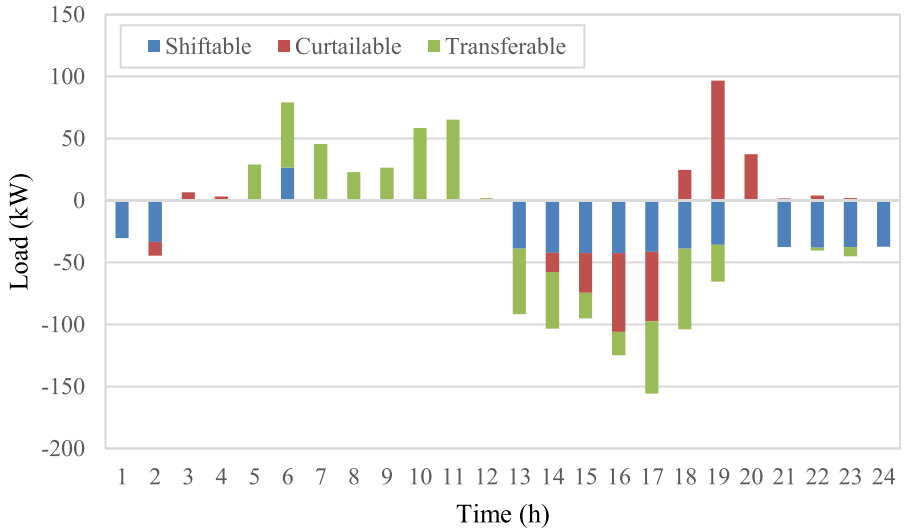

Fig. 7. Different load control schemes during restoration process in case 2.

Fig. 7 displays the hourly reaction of transferable, curtailable, and shiftable loads. A comparison of the graph in Fig. 7 with that of with Fig. 5 shows that fewer DRs have been used in case 2 compared to case 1, which is due to simultaneous consideration of cost and load restoration within the proposed multi-objective function optimization. In addition, the most frequently used program corresponds to the shiftable load type as shown in Fig. 7. For example, at 17 o'clock, the shiftable, curtailable and transferable loads are 41.4, 55.9 and 58.5, respectively.

Fig. 8 shows the hourly graph of power generation by DGs. Accordingly at the early morning hours, the generation is reduced. This reduction is due to the low level of load in these hours while the upper bound limitation of 50% for load transferring does not allow further

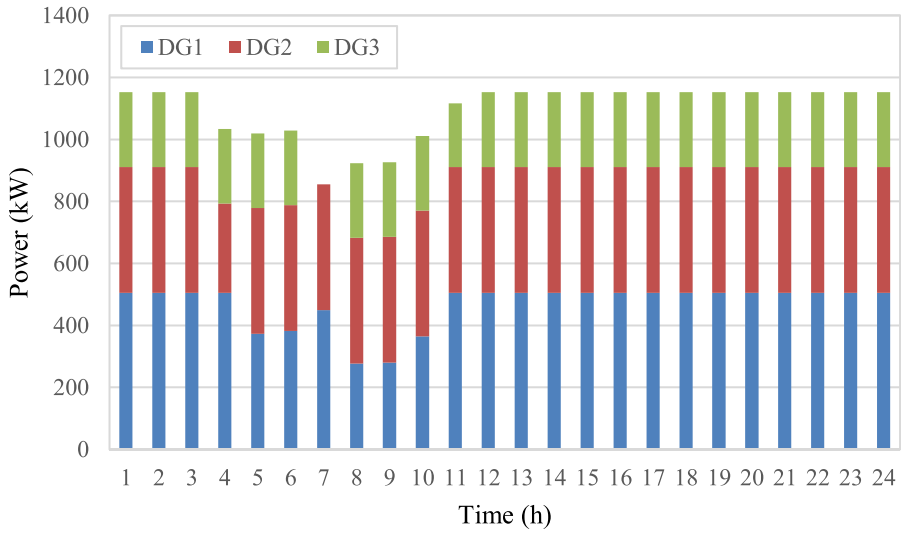

Fig. 8. Power generation by DGs in IEEE 37-bus test system in case 2.

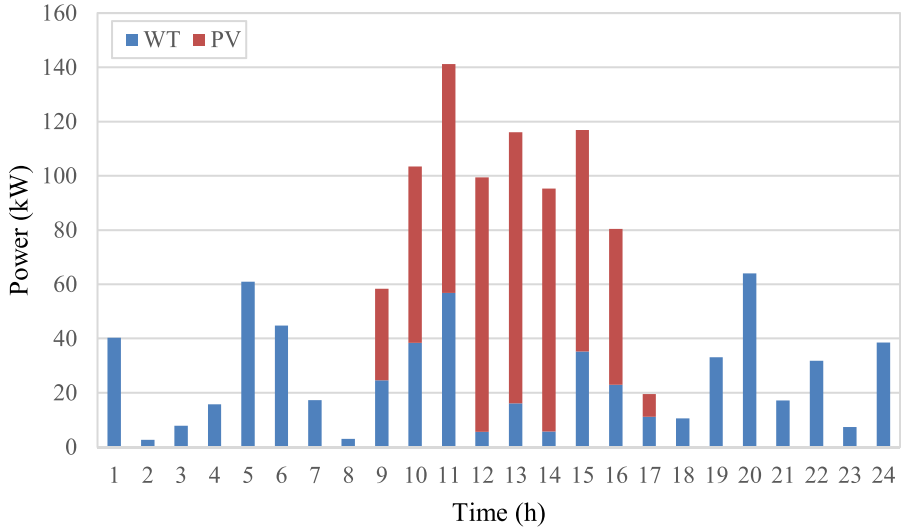

Fig. 9. Power generation by wind-based and PV units in IEEE 37-bus test system in case 2.

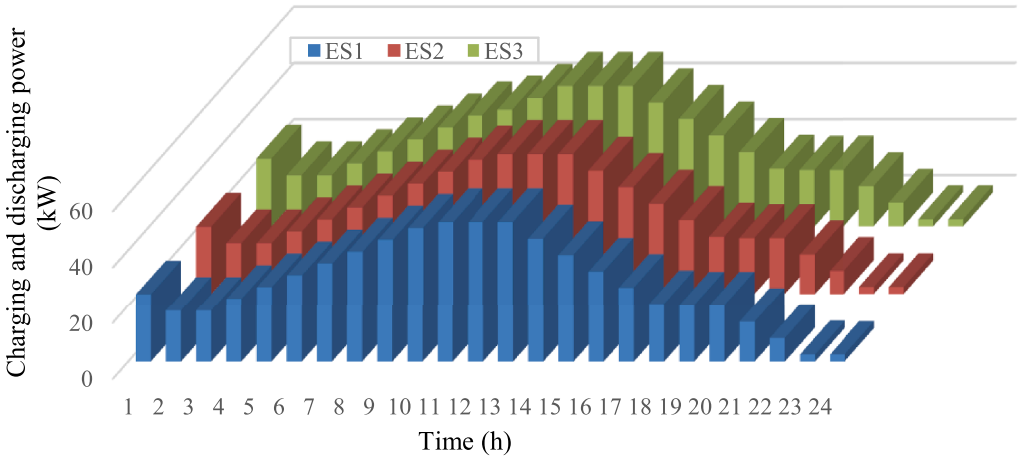

Fig. 10. The charging/discharging power of storage units in IEEE 37-bus distribution network in case 2.

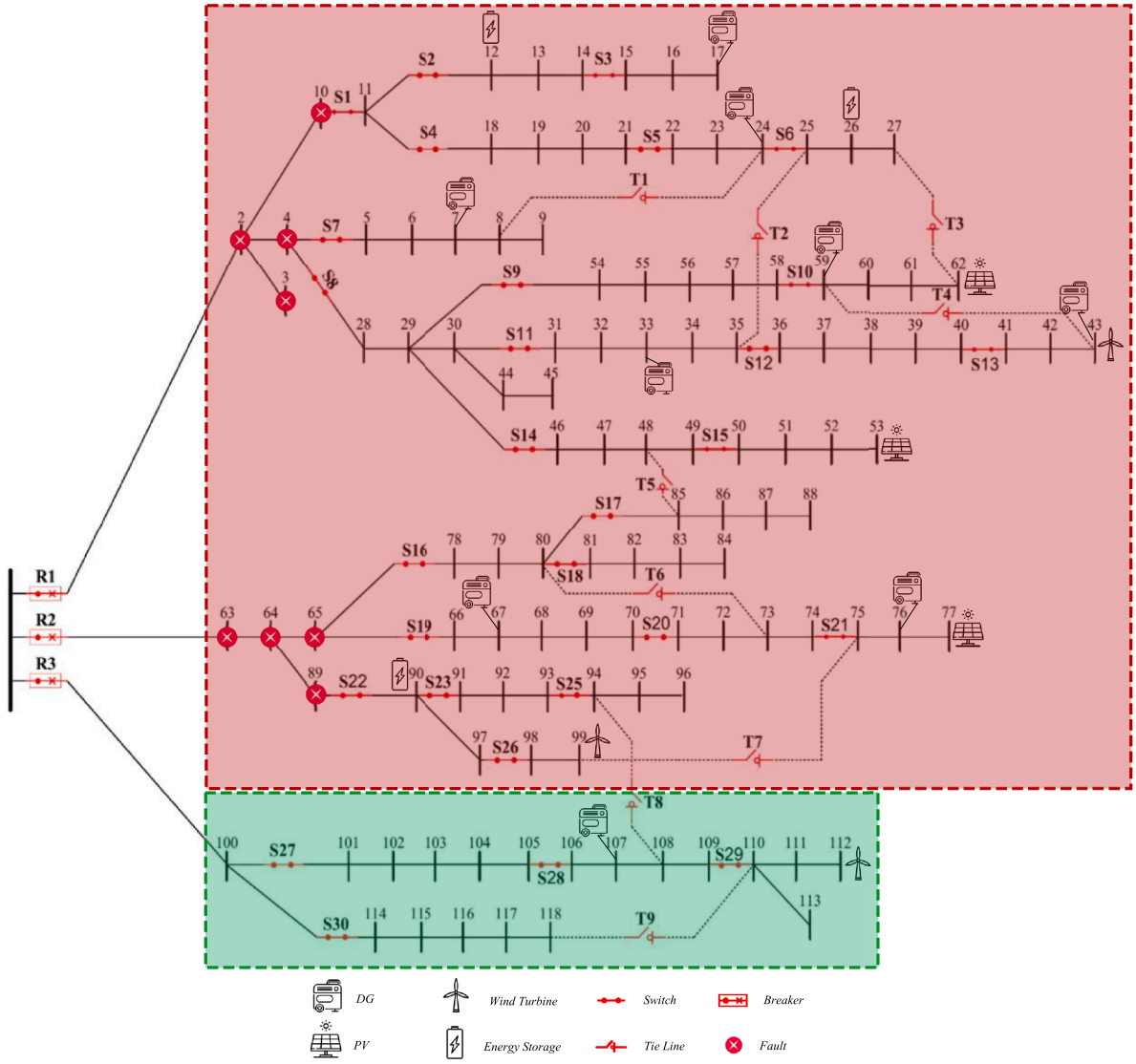

Fig. 11. The modified 118-bus distribution network at the event onset.

Table 7
Pay-off table of the ε-constraint method for 118-bus distribution network.

Scheduling objective function	Load shedding (kW)	Operational cost ($)
Load shedding minimization	177,529.9	11,790.67
Operational cost minimization	225,751.2	6812.053

utilization of DG capacity. Furthermore, all renewable units in the network are used in this case. Fig. 9 shows the hourly graph of generation by wind-based and PV units.

The charging/discharging power of storage units is shown in Fig. 10. According to this figure, storage units are charged in early hours and discharged in peak hours as rationally expected.

Table 8
Detailed Pareto solution for 118-bus distribution network.

Iteration number	Load shedding (kWh) Load	Restoration cost ($) Cost	Membership degree First objective function (μ_1) mu1	Membership degree Second objective function (μ_2) m2	Restoration cost limit (epsilon) Limit (Epsilon)	Minimum membership degree min(mu1,mu2)
Iter01	225,691.40	6812.05	0.00124	1	6812.0531	0.001240
Iter02	219,446.70	7309.91	0.13074	0.9	7309.9144	0.130741
Iter03	213,205.30	7807.77	0.26017	0.8	7807.7757	0.260173
Iter04	207,187.30	8305.63	0.38497	0.7	8305.6370	0.384974
Iter05	201,275.20	8803.49	0.50757	0.6	8803.4983	0.507576
Iter06	196,196.50	9301.36	0.61289	0.5	9301.3596	0.5
Iter07	190,611.40	9799.22	0.72871	0.4	9799.2209	0.4
Iter08	185,251	10,297.08	0.83988	0.3	10,297.0822	0.3
Iter09	180,491.40	10,794.94	0.93858	0.2	10,794.9435	0.2
Iter10	178,629.90	11,292.80	0.95856	0.1	11,292.8048	0.1
Iter11	177,529.90	11,595.42	1	0.039218	11,790.6662	0.039217

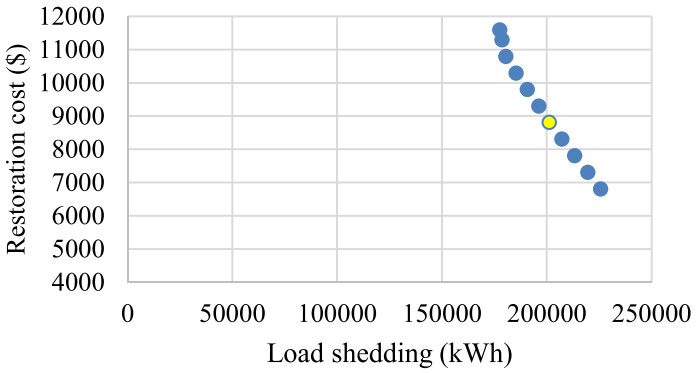

Fig. 12. Pareto-optimal solution for the 118-bus distribution network.

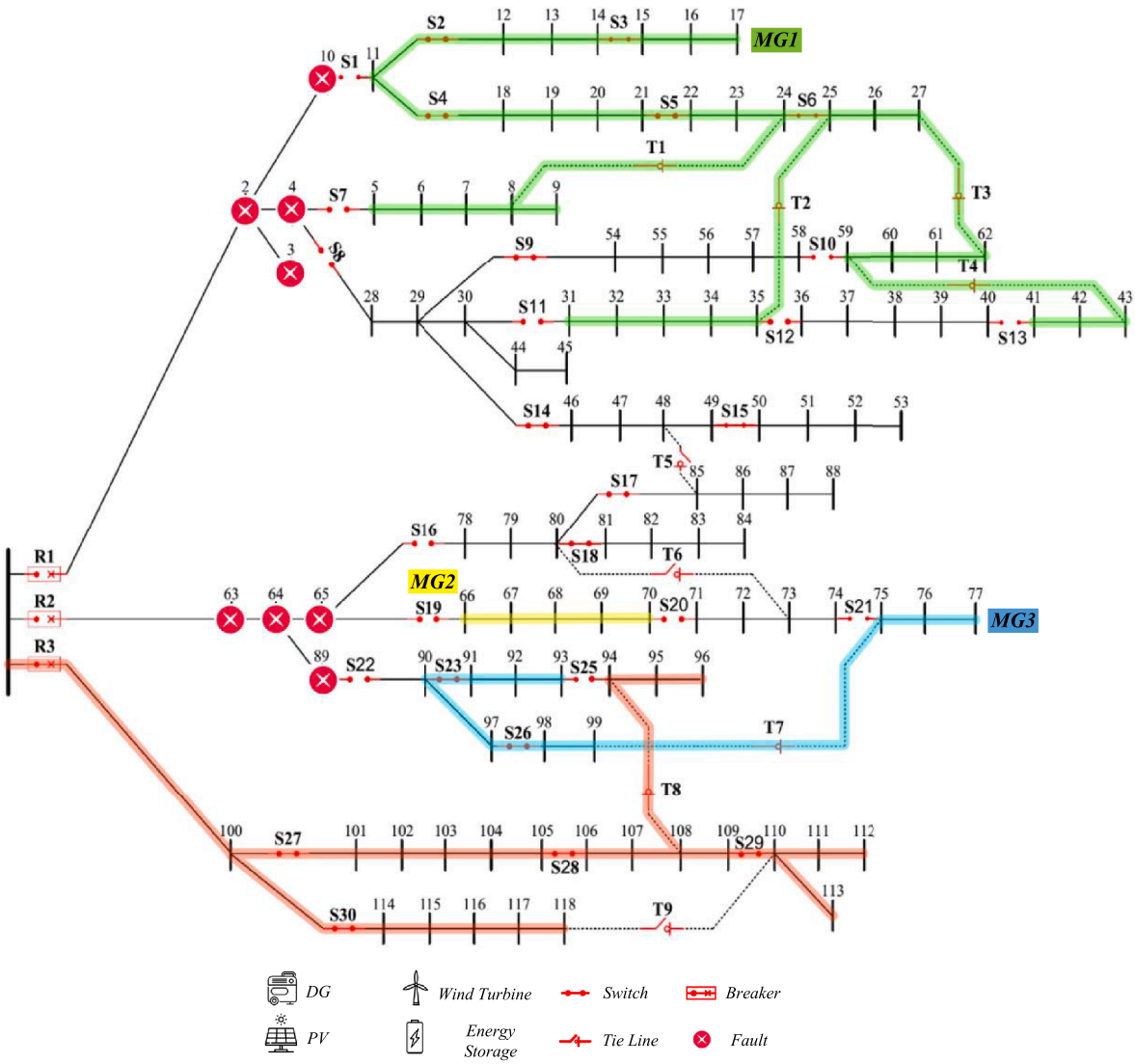

Fig. 13. MG formation post the event at the Pareto point for 118-bus distribution network.

4.2. 118-bus distribution network

The structure of 118-bus network and locations of generation and storage units are shown in Fig. 11. This network has 118 buses, 117 transmission lines, and 9 tie lines shown as dotted lines in Fig. 11. DGs at buses 17, 24, 59, 67, 76, and 107 are considered as master units with the capability of voltage-frequency control and MG formation. Moreover, 3 energy storage units have been considered for the test network. The capacity of PV, wind-based, and energy storage units are 50 kW, 100 kW, and 500 kWh, respectively. More detailed data for the network lines and buses can be found in (Ghasemi et al., 2021).

The structure of the test system after the event onset is illustrated in

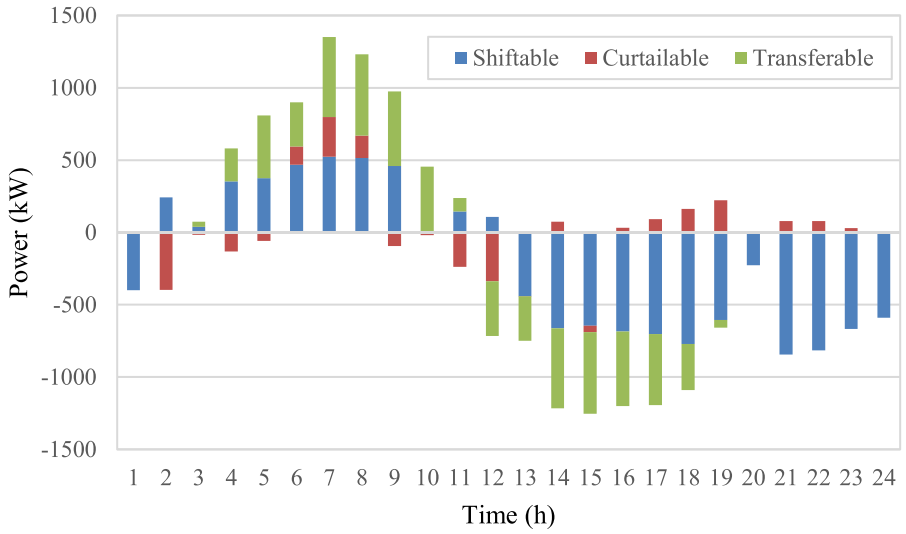

Fig. 14. Different load control schemes for 118-bus distribution network during restoration process.

Table 9
Results of sensitivity analysis for 118-bus distribution network.

Scenario	1	2	3	4	5	6	7	8
Tie line	✓	×	✓	✓	✓	×	×	×
ESS, WT, PV, Slave DG	✓	✓	×	✓	×	×	✓	×
DR	✓	✓	✓	×	×	✓	×	×
Load shedding (kWh)	201,275.2	253,018.5	217,978.4	225,751.2	243,236.3	255,180.6	264,195.6	267,429.8
Operation cost ($)	8803.49	4637.94	7456.44	6812.05	5427.26	4536.80	3722.47	3491.78
Resiliency index	0.498	0.380	0.460	0.442	0.402	0.375	0.355	0.347
Number of MGs	3	4	3	2	3	3	3	4
Solving time (Min)	42	12	32	20	24	8	8	4

Fig. 11. Due to the imposed fault, buses 100 to 118 are still connected to the upstream grid and the rest of the network is disconnected from the main grid.

The two-objective function model is implemented on the 118-bus distribution network. The front table is first computed and displayed in Table 7. The number of solution points and variation steps for the maximum level of constraint are similar to those of the 37-bus distribution network. The results of this case are shown in Table 8 and Fig. 12.

According to Table 8, the minimum membership degree at Point 5 is at its maximum. In this case, the restoration cost, load shedding, and resilience index are 8803.498 $, 201,275.2 kWh, and 49.84%, respectively. As shown in Fig. 12, the Pareto solution is the best trade-off between the two objective functions. Given the selected optimal Pareto point, the network structure is illustrated in Fig. 13.

As depicted in Fig. 13, three MGs are formed in feeders 1 and 2 in the restoration process. In addition, feeder 3 is connected to the upstream network and buses 94, 95, and 96 are supplied from feeder 3 by closing tie line T8. The resilience index for each of the MGs 1, 2, and 3 are 0.95, 1, and 1, respectively. In addition, the network resilience index is 49.84%. The hourly graph of using load control for transferable, curtailable, and shiftable loads is shown in Fig. 14. As depicted in this figure, the most frequently used program corresponds to the shiftable load type.

4.2.1. Sensitivity analysis

A sensitivity analysis is conducted here to investigate the impact of significant factors on the results presented in the previous sections. The scenarios and results of the sensitivity analysis are given in Table 9. Scenario 1 is considered as the base scenario in which tie lines, DERs, and demand response programs are employed simultaneously. According to the results of sensitivity analysis, the absence of tie lines imposes the largest increase on load shedding due to limitation for forming MGs whereas the resilience index in scenario 2 decreases around 23% in comparison with scenario 1.

5. Conclusion

A post-event restoration scheme was proposed for distribution systems after an HR event using MG formation, distributed energy resources, and demand response programs including transferable, curtailable, and shiftable loads. A multi-objective optimization model was proposed considering two conflicting objectives including operation cost and load shedding to improve the resilience of the electricity distribution network. Using ε-constraint method, the proposed model was solved to achieve the best Pareto front solution using a fuzzy-based method. The presented model was numerically examined on two standard test networks. According to the results, the network resilience index of 37-bus distribution system decreased around 3.2% as the restoration cost is considered in the two-objective model. In addition, due to simultaneous consideration of cost and load restoration within the proposed multi-objective function optimization, fewer DRs were used in the multi-objective model compared to single-objective one. The efficiency and applicability of the proposed restoration model was verified on 118-bus distribution system as well. The results of sensitivity analysis on this network confirmed that the absence of tie lines imposes the largest increase on the amount of load shedding. Also, as the demand response programs were used in this test system, the network resilience index increased around 12%. The simulation results showed that the model can make full benefit of smart grid facilities such as MGs formation, distributed energy resources, and demand response programs to rapidly restore the distribution system post the event. In future works,

we will focus on the resilience of energy hub systems through the stochastic optimization model after an HR event.

Declaration of Competing Interest

The authors declare that they have no known competing financial interests or personal relationships that could have appeared to influence the work reported in this paper.

References

https://www.dropbox.com/s/za05ho6owggrljo/Scenario%20Data.xlsx?dl=0.

Alizadeh, M., Jafari-Nokandi, M., & Shahabi, M. (2020). Resiliency-oriented islanding of distribution network in the presence of charging stations for electric vehicles. *International Transactions on Electrical Energy Systems, 30(12)*, E12670.

Amirioun, M. H., Aminifar, F., & Shahidehpour, M. (2018). Resilience-promoting proactive scheduling against hurricanes in multiple energy carrier microgrids. *IEEE Transactions on Power Systems, 34*(3), 2160–2168.

Bajpai, P., Chanda, S., & Srivastava, A. K. (2016, November 1). A novel metric to quantify and enable resilient distribution system using graph theory and choquet integral. *IEEE Transactions on Smart Grid, 9*(4), 2918–2929.

Biswas, S., Singh, M. K., & Centeno, V. A. (2021). Chance-constrained optimal distribution network partitioning to enhance power grid resilience. *IEEE Access, 9*, 42169–42181.

Borghei, M., & Ghassemi, M. (2021). Optimal planning of microgrids for resilient distribution networks. *International Journal of Electrical Power & Energy Systems, 128*, Article 106682.

Bynum, M., Castillo, A., Watson, J. P., & Laird, C. D. (2019, July). Evaluating demand response opportunities for power systems resilience using MILP and MINLP formulations. *AIChE Journal, 65*(7), E16508.

Chévez, P., Barbero, D., Martini, I., & Discoli, C. (2017). Application of the k-means clustering method for the detection and analysis of areas of homogeneous residential electricity consumption at the Great La Plata region, Buenos Aires, Argentina. *Sustainable Cities and Society, 32*, 115–129.

Ding, T., Lin, Y., Bie, Z., & Chen, C. (2017, August 1). A resilient microgrid formation strategy for load restoration considering master-slave distributed generators and topology reconfiguration. *Applied Energy, 199*, 205–216.

Farsangi, A. S., Hadayeghparast, S., Mehdinejad, M., & Shayanfar, H. (2018). A novel stochastic energy management of a microgrid with various types of distributed energy resources in presence of demand response programs. *Energy, 160*, 257–274.

Ghasemi, M., Kazemi, A., Bompard, E., & Aminifar, F. (2021, November 1). A two-stage resilience improvement planning for power distribution systems against hurricanes. *International Journal of Electrical Power & Energy Systems, 132*, Article 107214.

Ghasemi, M., Kazemi, A., Mazza, A., & Bompard, E. (2021, July). A three-stage stochastic planning model for enhancing the resilience of distribution systems with microgrid formation strategy. *IET Generation, Transmission & Distribution, 15*(13), 1908–1921.

Gholami, A., Shekari, T., Amirioun, M. H., Aminifar, F., Amini, M. H., & Sargolzaei, A. (2018). Toward a consensus on the definition and taxonomy of power system resilience. *IEEE Access, 6*, 32035–32053.

Gilani, M. A., Kazemi, A., & Ghasemi, M. (2020, January 15). Distribution system resilience enhancement by microgrid formation considering distributed energy resources. *Energy, 191*, Article 116442.

Hafiz, F., Chen, B., Chen, C., de Queiroz, A. R., & Husain, I. (2019, March 28). Utilising demand response for distribution service restoration to achieve grid resiliency against natural disasters. *IET Generation, Transmission & Distribution, 13*(14), 2942–2950.

Hemmati, R., Mehrjerdi, H., & Nosratabadi, S. M. (2021). Resilience-oriented adaptable microgrid formation in integrated electricity-gas system with deployment of multiple energy hubs. *Sustainable Cities and Society, 71*, Article 102946.

Momen, H., Abessi, A., & Jadid, S. (2020). Using EVs as distributed energy resources for critical load restoration in resilient power distribution systems. *IET Generation, Transmission & Distribution, 14*(18), 3750–3761.

Momen, H., Abessi, A., Jadid, S., Shafie-khah, M., & Catalão, J. P. (2021). Load restoration and energy management of a microgrid with distributed energy resources and electric vehicles participation under a two-stage stochastic framework. *International Journal of Electrical Power & Energy Systems, 133*, Article 107320.

Mousavizadeh, S., Haghifam, M. R., & Shariatkhah, M. H. (2018, February 1). A linear two-stage method for resiliency analysis in distribution systems considering renewable energy and demand response resources. *Applied Energy, 211*, 443–460.

Munikoti, S., Natarajan, B., Jhala, K., & Lai, K. (2021). Probabilistic voltage sensitivity analysis to quantify impact of high PV penetration on unbalanced distribution system. *IEEE Transactions on Power Systems, 36(4)*, 3080–3092.

Najafi, J., Peiravi, A., & Guerrero, J. M. (2018). Power distribution system improvement planning under hurricanes based on a new resilience index. *Sustainable Cities and Society, 39*, 592–604.

Nojavan, S., Majidi, M., & Zare, K. (2018). Optimal scheduling of heating and power hubs under economic and environment issues in the presence of peak load management. *Energy Conversion and Management, 156*, 34–44.

Panteli, M., Mancarella, P., Trakas, D. N., Kyriakides, E., & Hatziargyriou, N. D. (2017). Metrics and quantification of operational and infrastructure resilience in power systems. *IEEE Transactions on Power Systems, 32*(6), 4732–4742.

Sedzro, K. S., Lamadrid, A. J., & Zuluaga, L. F. (2017, August 29). Allocation of resources using a microgrid formation approach for resilient electric grids. *IEEE Transactions on Power Systems, 33*(3), 2633–2643.

Sedzro, K. S., Shi, X., Lamadrid, A. J., & Zuluaga, L. F. (2018, December 17). A heuristic approach to the Post-disturbance and stochastic pre-disturbance microgrid formation problem. *IEEE Transactions on Smart Grid, 10*(5), 5574–5586.

Shi, Q., Li, F., Olama, M., Dong, J., Xue, Y., Starke, M., et al. (2021). Post-extreme-event restoration using linear topological constraints and DER scheduling to enhance distribution system resilience. *International Journal of Electrical Power & Energy Systems, 131*, Article 107029.

Song, T., Li, Y., Zhang, X. P., Wu, C., Li, J., Guo, Y., et al. (2020). Integrated port energy system considering integrated demand response and energy interconnection. *International Journal of Electrical Power & Energy Systems, 117*, Article 105654.

Xu, Y., Liu, C. C., Schneider, K. P., Tuffner, F. K., & Ton, D. T. (2016, July 14). Microgrids for service restoration to critical load in a resilient distribution system. *IEEE Transactions on Smart Grid, 9*(1), 426–437.

Yuan, H., Li, F., Wei, Y., & Zhu, J. (2016, July 27). Novel linearized power flow and linearized OPF models for active distribution networks with application in distribution LMP. *IEEE Transactions on Smart Grid, 9*(1), 438–448.

Zadsar, M., Haghifam, M. R., & Larimi, S. M. (2017, July 21). Approach for self-healing resilient operation of active distribution network with microgrid. *IET Generation, Transmission & Distribution, 11*(18), 4633–4643.

Zeynali, S., Rostami, N., Ahmadian, A., & Elkamel, A. (2021). Stochastic energy management of an electricity retailer with a novel plug-in electric vehicle-based demand response program and energy storage system: A linearized battery degradation cost model. *Sustainable Cities and Society, 74*, Article 103154.

Zhu, J., Yuan, Y., & Wang, W. (2020, March 1). An exact microgrid formation model for load restoration in resilient distribution system. *International Journal of Electrical Power & Energy Systems, 116*, Article 105568.